Adsorption (2014) 20:147–156
DOI 10.1007/s10450-013-9559-7

High-rate and high-density gas separation adsorbents and manufacturing method

Jian Zheng · Philip A. Barrett · Steven J. Pontonio · Neil A. Stephenson · Preeti Chandra · Persefoni Kechagia

Received: 8 February 2013 / Accepted: 26 June 2013 / Published online: 23 July 2013

Abstract High-rate and high-density gas separation adsorbents used in vacuum pressure swing adsorption (VPSA) processes are described. Agglomerated zeolite Li–LSX compositions made using colloidal silica binding agents and having improved nitrogen pore diffusivity compared to like compositions prepared with traditional clay binders, are also described. Preparation methods for the colloidal silica-bound adsorbents are described together with their characterization by mercury (Hg) porosimetry, scanning electron microscopy (SEM) and low dead-volume breakthrough testing, from which the pore diffusivity is obtained. In this article, we show how the location and dispersion of the colloidal silica binding agent within the agglomerated zeolite particle yields pore-architectures that resemble "state-of-the-art" binderless adsorbents. In addition, we use VPSA process simulations to show that the best process performance is achieved by the combination of high-rate and high-density adsorbent properties.

Keywords Adsorbent kinetics · Adsorbent density · Adsorbent characterization · Li–LSX zeolite · Colloidal binder · Oxygen VPSA

1 Introduction

Air separation is an important industrial unit operation and can be accomplished using adsorption processes such as pressure swing adsorption (PSA) and vacuum pressure swing adsorption (VPSA). In PSA and VPSA processes, compressed air is pumped through a fixed bed of an adsorbent exhibiting an adsorptive preference for one of the main constituents, typically N_2, whereby an effluent product stream enriched in the lesser-adsorbed constituent (typically O_2) is obtained (Ruthven 1984; Kumar 1996; Yang 1997). Compared to cryogenic processes, adsorption processes for air separation are carried out at ambient level temperature, require relatively simple equipment, and are easy to maintain. Adsorption processes, however, have lower product purity and recovery; thus, improvements in these processes remain important goals. One principal means of improvement is the discovery and development of better adsorbents.

Historically, Na-exchanged X and other zeolite types, including Ca-exchanged A, were the adsorbents of choice for many of the first generation adsorptive air separation processes (Coe and Kuznicki 1984; Gaffney 1996). More recently, Li-exchanged X zeolite, especially with low silica-to-alumina ratio, such as Li–LSX, and higher Li exchange levels was introduced (Chao 1989; Weston et al. 2007). These Li–LSX adsorbents have become state-of-the-art for most VPSA processes.

A number of studies have described many of the key structural characteristics and properties of the Li–LSX adsorbent. These include accessible cation positions and mobility, adsorption energetics for O_2 and N_2 as well as, the impact of contaminants, including moisture, on the adsorption capacity (Feuerstein and Lobo 1998; Shen et al. 2001; Hutson et al. 2000). However, the detailed commercial manufacturing processes to produce the Li–LSX adsorbent in quantity for industrial gas separation usage remains less well-defined with most adsorbent manufacturers having unique manufacturing schemes. In particular, the agglomeration processes to form the Li–LSX into

J. Zheng · P. A. Barrett · S. J. Pontonio · N. A. Stephenson · P. Chandra · P. Kechagia (✉)
Praxair Inc., 175 East Park Drive, Tonawanda, NY 14150, USA
e-mail: persefoni_kechagia@praxair.com

shaped particles, especially beads, is often described as more of an art than a science.

One way to improve the adsorption properties of the Li–LSX is to enhance the mass transfer rate of adsorbent agglomerates by fine-tuning the bead forming and associated processes. With a fast mass transfer rate, one can reduce the cycle time and, in turn, lower the power consumption and increase the adsorbent productivity in PSA/VPSA systems and processes (Sircar 1992; Ackley 2000; Todd and Webley 2005). One strategy to increase the mass transfer rate of an agglomerated adsorbent particle is to reduce the particle size of adsorbent aggregates (Alpay et al. 1994; Wankat 1987; Ackley and Smolarek 2004). This will increase the adsorption/desorption kinetics by reducing the path length needed for adsorbates to travel through the rate-limiting macropores of the agglomerated adsorbent. Reducing the particle size however, has its limitations: higher pressure drop and increased risk of fluidization in unconstrained adsorption beds quickly become issues for adsorption process and system designs. Moreover, containment and manufacturing of small particle sized agglomerates represent other drawbacks that need to be resolved.

A preferred approach to increase the adsorption kinetics is to increase the pore diffusivity (Ackley and Leavitt 2002). This is technically more challenging than simply reducing the particle size of the agglomerated adsorbent particles, but if achieved, offers the greatest benefit. One way to improve the pore diffusivity of Li–LSX adsorbents is to produce agglomerated particles that are essentially binder-free using a caustic digestion process to convert zeolitizable clay binders (e.g., kaolin) into active zeolite adsorbent (Harada and Hirano 2001; Plee 2001; Chao and Pontonio 2002). This method also facilitates the removal of clay layers that block the Li–LSX adsorbent macropores (Chao and Pontonio 2002). A well-known drawback of the caustic digestion approach is the higher manufacturing cost involved in carrying out this process at commercial scales. In this article we describe an alternative and unique way of producing higher mass transfer rate Li–LSX agglomerated adsorbents by using colloidal binding agents, such as colloidal silica, instead of traditional clays (Zheng et al. 2012).

A crucial adsorbent property that affects process performance in commercial PSA/VPSA systems is its physical strength. Typically, the adsorbent density is inversely proportional to its porosity, meaning that higher porosity of certain adsorbent, albeit relating to higher intrinsic adsorption rate, could naturally result in lower density which reduces its physical strength. Moreau and Barbe (1997) concluded that when the porosity of the adsorbent increased, the VPSA system performance significantly improved. However, they did not mention the physical strength of their adsorbents.

We show herein that colloidal silica-bound Li–LSX adsorbents can be engineered through appropriate forming recipes and methods to possess unique macropore structures that exhibit a high mass transfer rate while maintaining high density as compared to clay-bound commercial materials. In terms of pore diffusivity, the colloidal silica-bound Li–LSX adsorbents can exhibit up to 120 % enhancement compared to the current state-of-the-art clay-bound Li–LSX adsorbents. In addition, the results of the impact of these novel adsorbents on the VPSA performance, which were obtained using process modeling techniques, are shared and discussed.

2 Experimental section

2.1 Sample preparation

Sample A is a commercial Li–LSX beaded adsorbent with an average particle size of 1.0 mm, manufactured by Zeochem LLC (Z10-05-03). It contains about 12 wt% clay binder, balance zeolite, and is ion-exchanged with approximately 96 % Li on a charge equivalents basis. The residual moisture content of Sample A, after activation under dry nitrogen purge at temperatures up to 400 °C, is less than or equal to 0.3 wt%.

Sample B is a Li–LSX adsorbent that was manufactured in the laboratory. It was prepared by mixing Na, K–LSX powder from Zeochem LLC with 7.0 wt% colloidal silica Ludox LS-30 and 3.0 wt% Methocel F4M (note that all weight percentages are expressed on a dry weight basis). The colloidal silica Ludox LS-30 was purchased from Dow Chemical and the Methocel F4M from Aqualon. Specifically, 2 kg of dry Na, K–LSX and 0.06 kg of Methocel F4M powders were mixed with 0.5 kg of Ludox LS-30 in a Hobart mixer for 1 h. The mixture was then transferred to a laboratory scale Nauta mixer, having an internal volume of about 1 ft^3, followed by the gradual addition of 0.83 kg water under constant mixing. Additionally, 0.18 kg of the above dry powder mixture was added back into the beads near the end of the forming process to control the bead size distribution to the desired 1.0 mm in average particle diameter. The entire bead forming, including the original powder mixing, took approximately 4 h. The product beads were air-dried overnight prior to calcination using a shallow tray method at temperatures up to 593 °C. The shallow tray calcination method used a General Signal Company Blue M Electric oven equipped with a dry air purge. Li exchange of the samples was carried out using a column ion exchange process. The Li exchange level was at least 98 % Li on a charge equivalents basis. Finally, the wet samples were dried and activated using equivalent conditions and method to the calcination process described above.

Sample C is a Li–LSX adsorbent manufactured again using the Nauta forming method, but this time at a larger semi-commercial scale. It was prepared by mixing Na, K–LSX powder from Zeochem LLC with 7.0 wt% colloidal silica Ludox LS-30 and 3.0 wt% Methocel F4M, all based on a dry basis. Specifically, 69 lbs. of dry Na, K–LSX, 17.25 lbs. Ludox LS-30 and 2.07 lbs. of Methocel F4M were mixed using a Littleford Day LS-150 plow mixer for 10 min. The mixture was then transferred to a semi-commercial scale Nauta processor, having an internal volume of about 7 ft^3, followed by the gradual addition of 57 lbs. of water under constant mixing. Two identical batches were processed separately, each over a three-hour period, and then combined. The products from these two batches were screened (as before to 1.0 mm in average particle diameter and air dried), calcined, and Li exchanged and activated using the processes and methods described above for Sample B.

2.2 Materials characterization

2.2.1 Isotherms

Pure component N_2 and O_2 isotherms were measured for each sample using the gravimetric method with a Sartorius MicroBalance. The isotherms were measured at three temperatures: 0, 27, and 47 °C. From these data, the Loading Ratio Correlation relationship (Yon and Turnock 1971) was used to extract the multi-component adsorption loading for both N_2 and O_2 on the adsorbent samples. The multi-component loading on the adsorbents was used for the simulation of the breakthrough experiment and also for the VPSA process model (see below).

2.2.2 Mercury porosimetry

Mercury (Hg) porosimetry measurements to determine the intraparticle void volume and adsorbent porosity were performed using a Micromeritics AutoPore IV instrument. Approximately, 1 g of sample was used for each measurement. The contact angle was fixed at 135° and intrusion and extrusion data were recorded over the pressure range from 0.5 psia to 61,000 psia.

2.2.3 Scanning electron microscopy (SEM)

The adsorbent beads were also characterized with Scanning Electron Microscopy (SEM), using a special sample preparation method designed to obtain a true cross-section of an adsorbent bead (Chao and Pontonio 2002). First, the adsorbent beads were immersed and set in a low viscosity epoxy resin. A polishing technique was then employed to expose approximately the mid-point of the collection of beads. Next, low temperature oxygen plasma was used to etch away the outer layer of epoxy and expose the adsorbent material once more prior to a final sample preparation step that involved spritzing the sample with gold to increase its conductivity. For the SEM analyses, a Jeol JSM-5600 SEM instrument was used, at least three beads of a given adsorbent sample were studied, and images were obtained at different magnifications. For the purposes of the images reproduced in this article, representative SEM pictures at 4,500X magnification are used to illustrate the key features of the adsorbent samples.

2.2.4 Breakthrough test

A custom-designed breakthrough test system and method developed by Fred Leavitt, the Low Dead Volume Test (LDVT), was employed to extract the kinetic characteristics of the adsorbents. This test system has been described in detail elsewhere (Ackley and Leavitt 2002).

This LDVT breakthrough test was performed in two, three-minute steps, in which the flow rate, pressure, and temperature of the feed gas remained constant. During this test, the temperature was maintained at 300°K, the pressure was 1.5 bar and the molar flux was controlled to 10 mol/m^2. The first step involved saturation of the adsorbent bed with the least selective component, O_2. In the second step, dry air was introduced to the bed with the more selectively adsorbed component, N_2, in the feed air displacing most of the pre-adsorbed O_2. The O_2 concentration profile as a function of time was recorded throughout the entire LDVT measurement. We have also conducted breakthrough experiments using synthetic air that contained N_2 and O_2 only, using different adsorbents than the ones described in this study. As a result, the fitting of the mass transfer parameter is emphasized in the range of O_2 concentrations from about 22 to 90 %.

The LDVT test was simulated using a computer process model developed on the Aspen Adsorption commercial modeling platform, and the mass transfer rate coefficients, k_i, for O_2 and N_2, were adjusted until the simulation breakthrough was in close agreement with the experimental data (Ackley and Leavitt 2002). The adsorption rate is calculated using the linear driving force model as described below in Sect. 2.3. It was discovered through simulation, and later verified through the experiment, that the LDVT test is not strictly isothermal. As a result, the model was modified to incorporate heat transfer at the wall of the bed. This is necessary since the heat generated during adsorption cannot be dissipated instantaneously, despite the isothermal bath and the small diameter of the adsorbent bed used in this test. As a result, the non-isothermal model introduces a lumped wall heat transfer coefficient as a third fitting parameter. However, this parameter, along with the

isotherm, affects the position of the breakthrough curve in time and has minimal influence upon the shape and steepness of the breakthrough characteristic.

After the mass transfer coefficients have been extracted, the effective pore diffusivity of the adsorbate, D_{pi}, was calculated using the following equation:

$$k_i = \frac{15\varepsilon_p(1-\varepsilon_b)D_{pi}}{r_p^2} \quad (1)$$

where ε_p is the void fraction inside the adsorbent particle, ε_b is the interparticle bed void fraction, and r_p is the average particle radius.

2.3 Process modeling

A detailed VPSA process model was developed using the commercial modeling platform Aspen Adsorption based on the governing material and energy balances (Ackley and Leavitt 2002). Process simulations enabled the impact of the adsorbent characteristics on the process performance to be determined. The model included a feed air inlet stream that entered an isentropic feed air compressor followed by a feed air aftercooler. During periods of unloading, the feed compressor was vented. Air then entered the adsorbent beds and oxygen is produced. Waste nitrogen and contaminants were removed from the adsorbent beds via a vacuum pump. The 12-step process performed by this VPSA system is outlined in Fig. 1. A two-bed VPSA configuration using these steps was used in the simulations. For all cases, the O_2 product purity was maintained at 90 % O_2 by adjusting the cycle time. The volume of the void spaces above and below the adsorbent bed inside the vessel was maintained constant, and the feed inlet superficial velocity to the adsorbent bed was maintained constant at 1.1 ft/s (measured at NTP conditions: 70 °F of temperature and 14.696 psia of pressure). The simulation was completed once a cyclic steady–steady was reached at the target purity of O_2 and at the given superficial inlet velocity. Also, the ratio of the pressure at the end of the adsorption step to that at the end of the desorption step was maintained constant and equal to 3.0, with the adsorption and desorption pressure typically at 1.5 and 0.5 bar, respectively. The depth of the adsorbent bed was 25 in. for all cases.

The linear driving force (LDF) model (Glueckaauf 1955) was used to calculate the adsorption rate:

$$\rho_b \frac{\partial \overline{w_i}}{\partial t} = k_i(c_i - \overline{c_{s_i}}) \quad (2)$$

where $\frac{\partial \overline{w_i}}{\partial t}$ is the adsorption rate, $\overline{w_i}$ is the average loading of the adsorbate (i), ρ_b is the packed density of the adsorbent in the bed, k_i is the mass transfer coefficient of the adsorbate (i), and c_i and c_{s_i} are average adsorbate gas phase concentrations in the bulk fluid and inside the particle in equilibrium with the adsorbate loading, respectively. The term in the brackets represents the concentration driving force. This representation of rate is directly related to the model for diffusion in solids, which incorporates diffusion represented by the Fickian model (Karger and Ruthven 1992). The model also used one-dimensional plug flow with negligible axial dispersion. Additional characteristics of the model included pressure drop, as determined by the Ergun Equation, and multicomponent isotherms as described above. A non-isothermal energy balance was used to account for heat transfer and the adsorbent vessel was treated as adiabatic.

3 Results and discussion

3.1 Material characterization

Figure 2(a) and (b) shows the isotherm data for pure component N_2 and O_2 respectively on the three samples of interest at 27 °C along with the fitting using the Loading Ratio Correlation relationship. The clay-bound Sample A has approximately 5 % lower N_2 capacity than the colloidal silica-bound Sample B, at a temperature of 27 °C and a pressure of 1.0 bar. This is expected since the Li exchange level was 96 % for Sample A and 98 % or higher for Sample B.

Figure 3 shows the pore size distribution of the commercial, clay-bound Sample A compared to the colloidal silica-bound Sample B, as characterized by Hg porosimetry at Hg intrusion pressures in the range of 18–45,000 psia. Both samples exhibit similar pore distributions with a distinct maximum at relatively large pore sizes. The vast majority of macropores in Sample A is in the range of 0.1–0.9 μm with a median pore diameter of 0.27 μm. In Sample B however, the majority of macropores span sizes from 0.3 to 2 μm with a median pore diameter of 0.65 μm. Hence, Sample B has larger macropores and a greater median pore diameter than Sample A, both of which are expected to positively affect the adsorption kinetics and increase the pore diffusivity of Sample B compared to Sample A. Another significant difference between the two samples is in the range of smallest measurable pore sizes from the Hg porosimetry technique, from about 0.02 to 0.1 μm, wherein the clay-bound Sample A has a larger fraction of small macropores compared to Sample B.

Figure 4 shows different SEM images of the clay-bound Sample A as compared to the colloidal silica-bound Sample B. There is visual evidence of clay particles (Sample A) in between the zeolite crystallites, blocking some of the macropores created by the stacking of the crystallites, and forming denser regions inside the clay-bound beads. In Samples B and C, where colloidal silica was used as binding

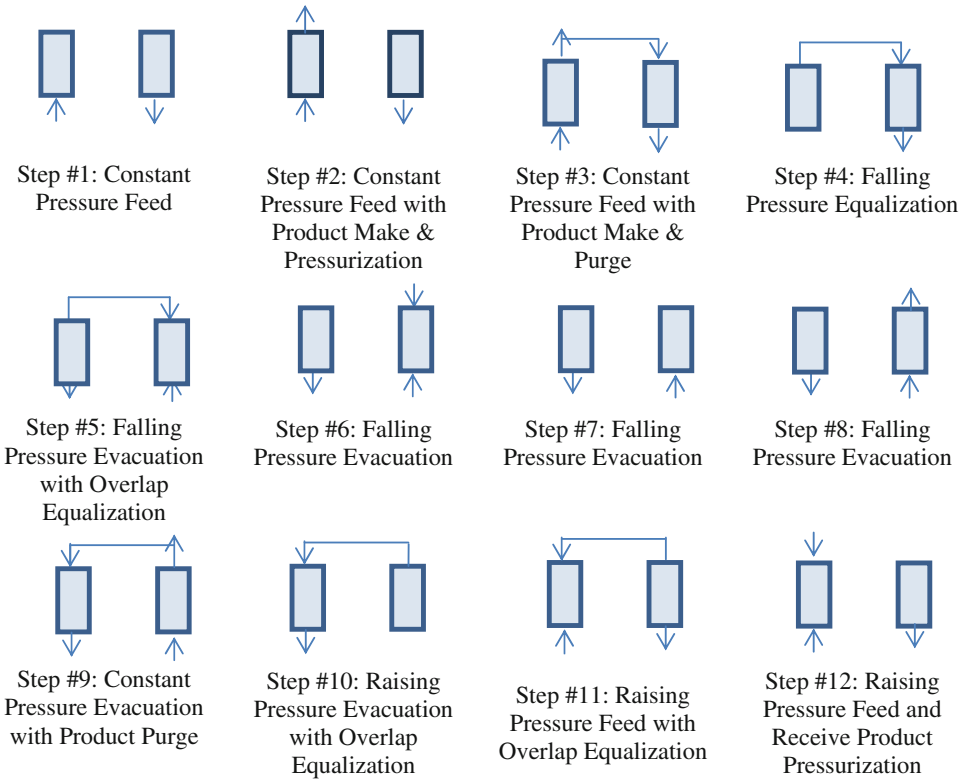

Fig. 1 Twelve-step VPSA process

agent, the macropores are essentially free of binding agent. In the SEM images, the zeolite crystallites are clearly visible, in contrast to the clay-bound Sample A. The size of the Na, K–LSX crystallites in the powder was 0.5–5.0 μm with the average around the 2.5 μm size as measured from SEM images. From these and other SEM images (not shown), it appears that the mechanism of binding between the colloidal silica and the clay is quite different. In the clay case, the commonality of large swathes of clay material suggests that the clay is preferentially binding to itself. In fact, in Fig. 4, small gaps between the clay and zeolite crystallites are commonly found supporting a lack of clay-zeolite binding. In view of these observations, it may be fair to describe the clay binding agent used for Sample A as a network style binder, wherein the zeolite crystallites are essentially encapsulated in a clay matrix. On the other hand, for the colloidal silica-bound sample there are not any areas of visible binding agent in between the zeolite crystallites. It could be that the resolution of the SEM images was not adequate to capture such structures. However, the lack of visible areas of binding agent in the macropores of the colloidal silica-bound sample suggests that the small silica particles are located more on the zeolite crystallite surfaces and provide a more contact point mode of binding. In the SEM images of the colloidal silica-bound Samples B and C, it often appears that the zeolite crystallites are more consolidated together, which may be a result of the "gluing" action of the small silica particles affixed to the zeolite crystallite surfaces. Despite the fact that the commercial Sample A contains 12 % of the Actigel clay, whereas the colloidal silica-bound Samples B and C contain only 7 % of Ludox LS-30, we believe that the network style of binding of the Actigel clay binder would have had affected the rate properties of the adsorbent in a very similar fashion even if Sample A was manufactured with 7 % of Actigel instead of 12 %. This conclusion is also supported by comparison of rate characteristics in Li–LSX adsorbent samples manufactured using either 10 % Actigel or 10 % Ludox LS-30 binder in Zheng et al. 2012. There, the colloidal silica-bound samples exhibited higher rate than the clay-bound samples.

In terms of the implications of these results on the kinetic properties described below, the absence of clay particles within the zeolite crystallite-derived macropores yields a more even pore structure in the colloidal silica-bound samples as evidenced by both the SEM and Hg porosimetry results. A network style of binding agent must, by default, reside within the macropores. This binding agent network will become part of the pore structure and thereby influence the adsorption kinetics. A contact point binder leaves the macropores open and instead influences the stacking of the zeolite crystallites to some extent. There is a lot of evidence from previous studies that for O_2 and N_2 adsorption on X-type agglomerated zeolites, such as Na, K–LSX and Li–LSX, the resistance in the macropores of the adsorbent particles is the rate controlling mechanism (Ackley et al. 2003; Karger and Ruthven 1992). From the

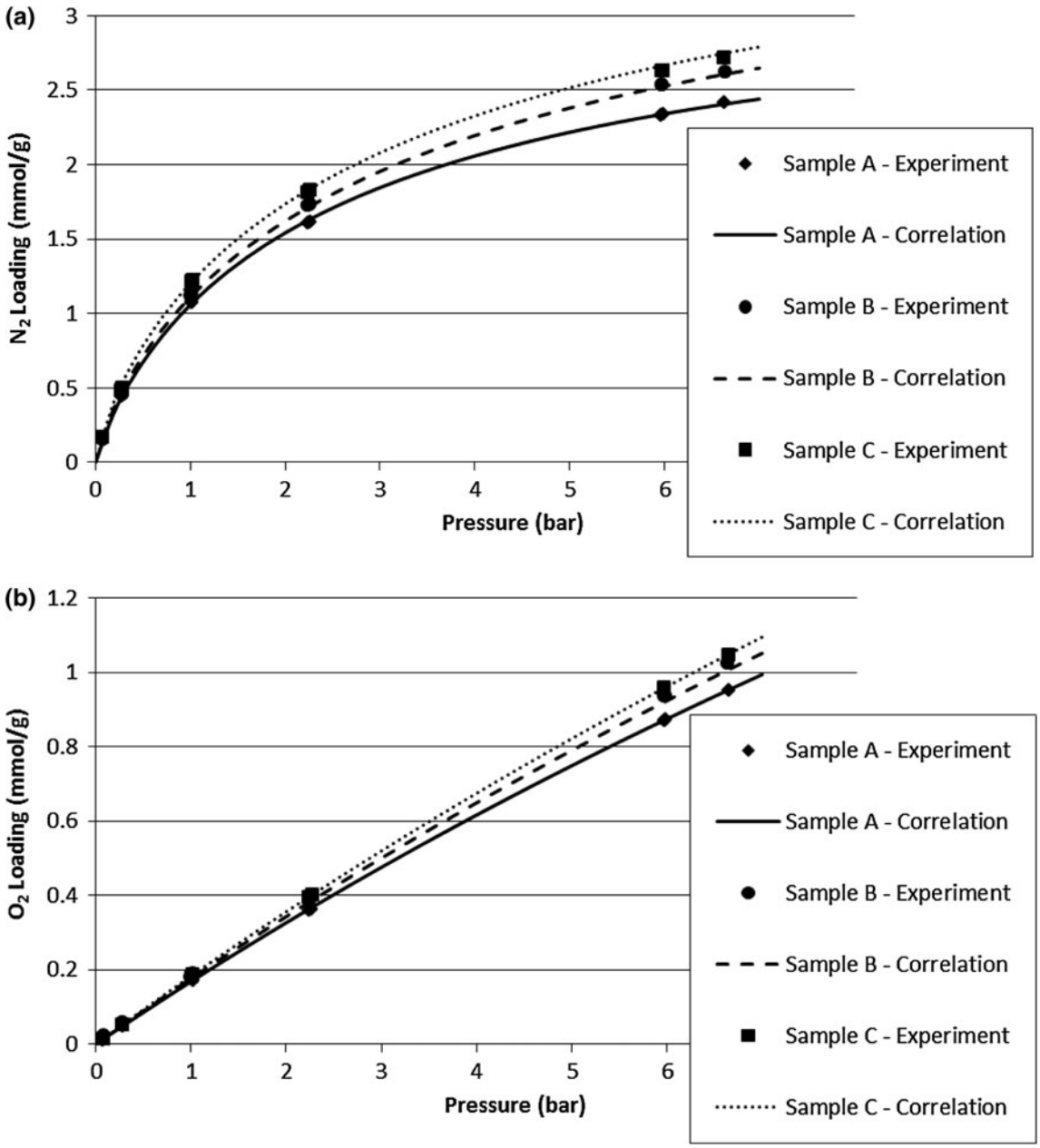

Fig. 2 Pure component isotherms for Samples A, B, and C at 27 °C. Plot **(a)** shows the isotherms for N_2 and plot **(b)** those for O_2. The *points* on the plots are the experimental values and the *lines* correspond to the prediction using the Loading Ratio Correlation realtionship

kinetic evaluation presented below, the colloidal silica-bound samples have higher N_2 pore diffusivity, compared to the clay-bound sample, supporting a preference for the contact-point style of binding agent.

3.2 Mass transfer coefficient and pore diffusivity analysis

As described in Sect. 2, the mass transfer coefficient for N_2, k_{N_2}, was determined by fitting the appropriate model to data from the breakthrough experiment. Figure 5 shows the experimental breakthrough curves and the model fit for the commercial clay-bound adsorbent, Sample A, and the laboratory colloidal silica-bound adsorbent, Sample B. The breakthrough tests were performed with dry air that included Ar, while in the breakthrough model, the Ar is lumped in with the O_2. This is the reason for the difference in the initial O_2 concentration between model and experiment prior to breakthrough when the time is less than 20 s (see Fig. 5). A good model fit to the breakthrough data was achieved when the mass transfer coefficient for N_2 was adjusted to 38 s^{-1} and 70 s^{-1} for Sample A and Sample B,

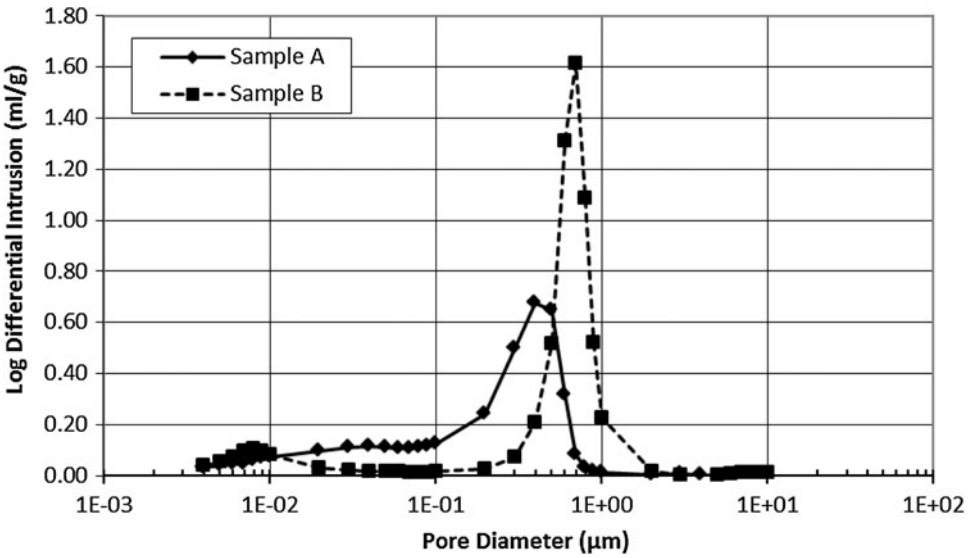

Fig. 3 Log differential intrusion volume versus pore diameter curves for clay-bound Sample A (*solid line* with *diamonds*) and colloidal silica-bound Sample B (*dashed line* with *squares*)

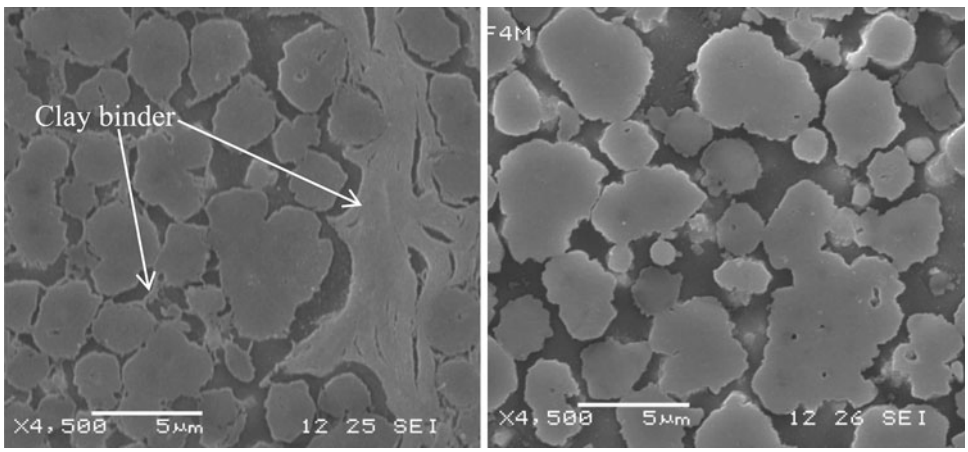

Fig. 4 SEM images of cross-sectional areas beads of Sample A (*left*) and Sample B (*right*)

respectively. The breakthrough front for Sample B is much sharper than that of Sample A (as depicted in Fig. 5), which is expected based on the high mass transfer coefficient of Sample B. The position of the breakthrough front reflects the capacity of the adsorbent bed to adsorb N_2. Hence, the breakthrough front for Sample A is positioned to the left of that of Sample B, since the clay-bound Sample A has approximately 5 % lower N_2 capacity than the colloidal silica Sample B, based on a pure component N_2 isotherm measured at a temperature of 300 °K and a pressure of 1.0 bar. The breakthrough front of Sample C is similar to that of Sample B, but even sharper. The breakthrough tests were repeated. What we found is that with low diffusivity samples, the variation in the mass transfer coefficient for N_2 is about 5 %. With higher diffusivity samples, this variation could be closer to 10 %. Even after consideration of these errors, the conclusions from this work remain unchanged. The limitation of the breakthrough method in calculating the kinetic parameters arises when the samples exhibit very high rates. In such cases, the front is so steep that a change in the O_2 concentration from 30 to 90 % happens in less than 0.5 s, and the number of points in the breakthrough front covering this range is limited by the response of the analyzer.

Then, the pore diffusivity for these adsorbents is calculated using Eq. 1. The results are shown in Table 1.

Differences in diffusivity also reflect slight differences in the average particle size of the samples and the bed void fraction. The average particle diameter for the three samples was in the range of 0.95–1.025 mm, while the bed void fraction range was 0.34–0.36.

As Table 1 shows, we were successful in increasing the pore diffusivity by 120 %, compared to the commercially available adsorbents, when the colloidal silica binder was used in the formation of the adsorbent instead of the traditional clay binder used in the commercial product. The pore diffusivity of the commercial Sample A is within the range of values that have been reported in the literature for commercial Na, K–LSX and Li–LSX agglomerated adsorbents. Furthermore, the pore diffusivity of Samples B

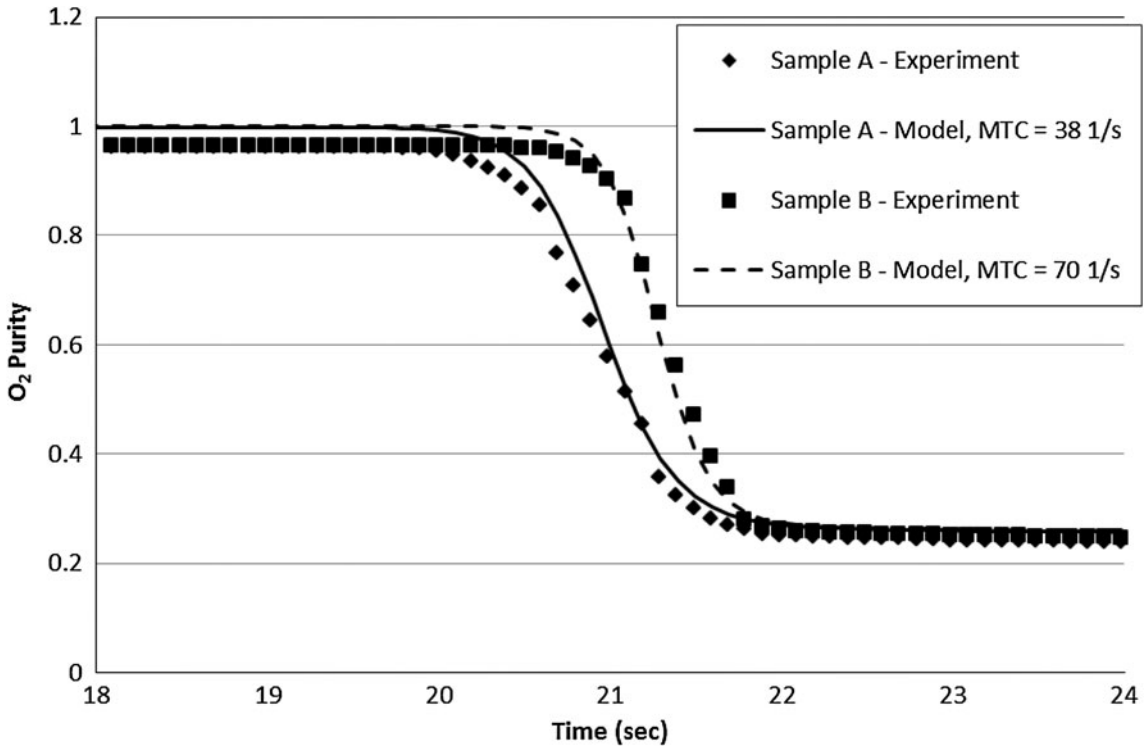

Fig. 5 Experimental results (*points*) and model prediction (*line*) of the LDVT breakthrough test using Sample A (*diamonds*, *solid line*) and Sample B (*squares*, *dashed line*)

Table 1 Mass transfer coefficient for N_2 and pore diffusivity of Li–LSX adsorbents

Adsorbent	N_2 mass transfer coefficient (s^{-1})	Pore diffusivity (m^2/s)	Particle density (g/cc)	Particle porosity (cc/cc)
Sample A	38	2.2×10^{-6}	0.88	0.39
Sample B	70	4.6×10^{-6}	0.88	0.41
Sample C	97	4.9×10^{-6}	0.78	0.46

and C is close to that of other high rate adsorbents that have been manufactured using a caustic digestion process (Ackley and Leavitt 2002). Both Samples B and C exhibit similar pore diffusivity, with Sample C having a slightly higher value. This increase in pore diffusivity is significant and is expected to have a positive impact on the process performance (Ackley and Leavitt 2002).

As mentioned previously, another important parameter for VPSA process performance is the density of the adsorbent particles. Table 1 shows the density and the porosity of the three different samples as measured by mercury porosimetry. Sample B has the same particle density as Sample A and very similar particle porosity to Sample A. The particle density of Sample C is approximately 11 % lower than Samples A and B. Both Samples B and C were manufactured using the Nauta forming method, as described in Sect. 2, and Sample C was manufactured before Sample B. Therefore, we were able to further optimize the forming method so that the density of Sample B approached the density of commercial samples. More specifically, we were able to decrease the total amount of water added in the forming step, and consequently increase the density of the adsorbent. In addition, the forming time for Sample B was longer than that of Sample C, which also played a role in increasing the density of Sample B.

Higher density adsorbents have the advantage of demonstrating greater physical strength for use in commercial PSA/VPSA processes for the production of O_2. The crush strength of the colloidal silica-bound samples is at least similar, if not better, to that of the conventional clay-bound samples as described in more detail in Zheng et al. 2012. It was found that the average crush strength of colloidal silica-bound adsorbents with average particle size of 1.0–1.5 mm, formed using a similar forming technique to the ones described in this study, was at least 0.9 lbf as measured by the single bead crush strength method. All crush strength measurements employed a Dr. Schleuniger Pharmatron Tablet Tester 8 M equipped with a 50 N load cell. Crush strength is measured on calcined products, using 40 beads from which the mean crush strength is calculated.

3.3 Process performance

The VPSA process model described above was used to understand the combined effect of the increase in pore diffusivity and the decrease in particle density on the process performance. The modeling results were used to guide the experimental efforts towards the development of adsorbents with higher rates. Therefore, the process modeling provided target values for the adsorbent characteristics, such as N_2 mass transfer coefficient and particle porosity, which were achieved experimentally to a large extent through the manufacturing of Sample B. Four cases were developed, as shown in Table 2, to reflect the effect of the material characteristics of interest: N_2 mass transfer coefficient, and particle porosity on the process performance. Therefore, for modeling purposes, the porosity of the adsorbent was varied from the typical porosity value of commercial samples, namely 0.38, to a porosity of 0.45, which is close to the value obtained for the colloidal silica-bound Sample C. The changes in porosity would in turn affect the particle density and the packed density of the adsorbent bed.

The material properties of the Base case correspond to Sample A. Case 1 uses properties that are very close to those of Sample B; Case 2 reflects the higher rate and the increase in particle porosity that were exhibited by Sample C. For comparison purposes, the N_2 mass transfer coefficient of the adsorbent of Case 1 and Case 2 was maintained the same. Finally, Case 3 reflects the effect of further increasing the rate while maintaining the particle porosity at the value of the commercial Sample A. As shown in Table 2, a comparison between the Base case and Cases 1 and 3 reveals that increasing the N_2 mass transfer coefficient from 38 to 60 s^{-1}, and finally to 80 s^{-1}, while maintaining the same particle porosity, is beneficial to the process performance in that the O_2 recovery, which is also a measure of productivity, was increased by approximately 2.5 and 3.7 % respectively. This is expected due to the increase of the adsorbent pore diffusivity. However, when comparing Case 2 to Case 1, we see that when the porosity of the adsorbent was increased, while its N_2 mass transfer coefficient was maintained constant, the process performance decreased. This is also expected since an increase in porosity results in a decrease of the active material for separation within the same volume of the adsorbent bed, and hence, a decrease in process performance. In addition, an increase in the porosity of the adsorbent results in an increase of the non-selective gas storage volume in the adsorbent bed; this decreases the separation efficiency and reduces overall product recovery. The unexpected result comes from comparing Case 2 to the Base case. Here, an increase in the N_2 mass transfer coefficient, accompanied by an increase in porosity, resulted in decreased process performance. This is the opposite to the teachings of Moreau and Barbe (1997). Therefore, a necessary requirement for the development of future superior adsorbents for VPSA processes is a higher N_2 mass transfer coefficient, and a prerequisite is to maintain the adsorbent particle porosity within the levels of traditional clay-bound adsorbents (i.e., in the range of 35–40 %). Based on this conclusion, the use of Sample B in a VPSA process is more advantageous than the use of Sample C, despite the higher N_2 mass transfer coefficient of the latter. This has also been verified by pilot tests of Samples A and C.

Table 2 VPSA process model inputs and performance metrics

	Base case	Case 1	Case 2	Case 3
Process inputs				
k_{N_2} (s^{-1})	38	60	60	80
Porosity (cc/cc)	0.38	0.38	0.45	0.38
Normalized recovery	1.0	1.025	0.991	1.037

4 Conclusions

In this paper, Li–LSX adsorbents prepared using traditional clay as well as colloidal silica binding agents have been studied both microscopically (at the individual particle level by a suite of characterization methods) and macroscopically at the packed bed level, by process modeling. We have shown through characterization methods namely Hg porosimetry, SEM, and a customized breakthrough test that Li–LSX adsorbent compositions, prepared appropriately using colloidal silica binding agents, are superior to the traditional clay-bound adsorbents in terms of their pore connectivity and N_2 pore diffusivity. More specifically, we have shown that the silica-bound adsorbents exhibit up to 120 % higher N_2 pore diffusivity compared to the clay-bound product. In addition, we have been able to translate this improvement in the adsorbent kinetics to a VPSA process performance benefit manifested by higher O_2 recovery using a rigorous VPSA process model. Our modeling results show that improvements to the adsorbent pore diffusivity at the expense of higher particle porosity offsets the VPSA process benefits obtained therefrom. The best process performance was achieved by adsorbent samples having a combination of improved N_2 pore diffusivity and at least equivalent particle porosity.

Acknowledgments The authors would like to thank the following individuals at Praxair for their contributions to the work described herein: Fred Leavitt and Mark Ackley are acknowledged for their constant support of the process, systems, and adsorbent developments related to the application of intensified gas separations. Bonnie Boudreau is thanked for her work in obtaining the SEM images and Hg porosimetry data for this study.

References

Ackley, M.W.: Multilayer adsorbent beds for PSA gas separation. US Patent 6,152,991 (2000)

Ackley, M.W., Leavitt, F.W.: Rate-enhanced gas separation. US Patent 6,500,234 (2002)

Ackley, M.W., Rege, S.U., Saxena, H.: Application of natural zeolites in the purification and separation of gases. Microporous Mesoporous Mater. **61**, 25–42 (2003)

Ackley, M.W., Smolarek, J.: Enhanced rate PSA process. US Patent 6,790,260 (2004)

Alpay, S., Kenney, C.N., Scott, D.M.: Adsorbent particle size effects in the separation of air by rapid pressure swing adsorption. Chem. Eng. Sci. **49**, 3059–3075 (1994)

Chao, C.C.: Process for separating nitrogen from mixtures thereof with less polar substances. US Patent 4,859,217 (1989)

Chao, C.C., Pontonio, S.: Advanced adsorbent for PSA. US Patent 6,425,940 (2002)

Coe, C.G., Kuznicki, S.M.: Polyvalent ion exchanged adsorbent for air separation. US Patent 4,481,018 (1984)

Feuerstein, M., Lobo, R.F.: Characterization of Li cations in zeolite LiX by solid-state NMR spectroscopy and neutron diffraction. Chem. Mater. **10**, 2197–2204 (1998)

Gaffney, T.R.: Porous solids for air separation. Curr. Opin. Solid State Mater. Sci. **1**, 69–75 (1996)

Glueckaauf, E.: Theory of chromatography. Part 10. Formulæ for diffusion into spheres and their application to chromatography. Trans. Faraday Soc. **51**, 1540–1550 (1955)

Harada, A., Hirano, S.: Method of adsorptive separation of carbon dioxide. EP 1142622 (2001)

Hutson, N.D., Zajic, S.C., Yang, R.T.: Influence of residual water on the adsorption of atmospheric gases in Li-X zeolite: experiment and simulation. Ind. Eng. Chem. Res. **39**, 1775–1780 (2000)

Karger, J., Ruthven, D.M.: Diffusion in Zeolites and Other Microporous Solids. Wiley, New York (1992)

Kumar, R.: Vacuum swing adsorption process for oxygen production—a historical perspective. Sep. Sci. Technol. **31**, 877–893 (1996)

Moreau, S., Barbe, C.: Process for the separation of mixtures of oxygen and of nitrogen employing an adsorbent with improved porosity. US Patent 5,672,195 (1997)

Plee, D.: Method for obtaining LSX zeolite. US Patent 6,264,881 (2001)

Ruthven, D.M.: Principles of Adsorption and Adsorption Processes. Wiley, New York (1984)

Shen, D., Bülow, M., Jale, S.R., Fitch, F.R., Ojo, A.F.: Thermodynamics of nitrogen and oxygen sorption on zeolites LiLSX and CaA. Microporous Mesoporous Mater. **48**, 211–217 (2001)

Sircar, S.: Polyvalent ion exchanged adsorbent for air separation. US Patent 5,084,075 (1992)

Todd, R.S., Webley, P.A.: Macropore diffusion dusty-gas coefficient for pelletised zeolites from breakthrough experiments in the O_2/N_2 system. Chem. Eng. Sci. **60**, 4593–4608 (2005)

Wankat, P.C.: Large-scale adsorption and chromatography. Ind. Eng. Chem. Res. **1**, 64–102 (1987)

Weston, K., Jaussaud, D., Chiang, R.L.: Lithium exchanged zeolite X adsorbent blends. US Patent 7,300,899 (2007)

Yang, R.T.: Gas Separation by Adsorption Processes. Imperial College Press, London (1997)

Yon, C.M., Turnock, P.H.: Multicomponent adsorption equilibria on molecular sieves. AIChE Symp. Ser. Adsorpt. Technol. **117**(67), 75–83 (1971)

Zheng, J., Pontonio, S.J., Stephenson, N.A., Barrett, P.A.: High rate and high crush strength adsorbents. US Patent 8,123,835 (2012)